

PAPER



Cite this: *Phys. Chem. Chem. Phys.*,
2023, 25, 32196

Size matters: asphaltenes with enlarged aromatic cores promote heat transfer in organic phase-change materials†

Artem D. Glova,^a Victor M. Nazarychev,^b Sergey V. Larin,^b
Andrey A. Gurtovenko^b and Sergey V. Lyulin^{*b}

Recent experiments and atomistic computer simulations have shown that asphaltene byproducts of oil refineries can serve as thermal conductivity enhancers for organic phase-change materials such as paraffin and therefore have the potential to improve the performance of paraffin-based heat storage devices. In this work, we explore how the size of the polycyclic aromatic cores of asphaltenes affects the properties of paraffin–asphaltene systems by means of atomistic molecular dynamics simulations. We show that increasing the size of the asphaltene core from 7–8 aromatic rings to ~20 rings drastically changes the aggregation behavior of asphaltenes. Instead of relatively small, compact aggregates formed by small-core asphaltene molecules, enlarged cores promote the formation of extended single-column structures stabilized in paraffin by asphaltene’s aliphatic periphery. Chemical modification of the asphaltenes by removing the periphery leads to the formation of bundles of columns. In contrast to small-core molecules, asphaltenes with enlarged cores do not suppress paraffin crystallization even at high filler concentrations. Remarkably, asphaltenes with enlarged aromatic cores are able to increase the thermal conductivity of liquid paraffin to a greater extent compared to their small-core counterparts. This effect becomes even more pronounced for modified asphaltenes without the aliphatic side groups. Overall, our computational findings suggest that asphaltenes with enlarged aromatic cores can significantly improve the performance of heat storage devices based on organic phase change materials.

Received 24th June 2023,
Accepted 8th November 2023

DOI: 10.1039/d3cp02953k

rsc.li/pccp

Introduction

Asphaltenes represent a group of waste materials produced by oil refineries.¹ Depending on its origin, oil can contain up to 20% of asphaltenes.^{2–4} As the global demand for oil is expected to reach approximately 100 million barrels per day in 2023 and continues to grow,⁵ the accumulation of asphaltene byproducts can become an essential environmental problem. A potential solution to this issue is to utilize asphaltenes for various applications such as the production of asphalt pavements,⁶ polymer composites,^{7–9} and solar cells.^{10–13} Thus, diversifying the applications of asphaltenes can aid in preventing their accumulation in the environment as well as in developing novel, high-value products.

Recent experiments and computer simulations have suggested that asphaltenes can be used as fillers for paraffin-based phase-change materials.^{14–16} These materials are promising for developing domestic thermal energy storage systems, but their low thermal conductivity limits their performance by reducing charging and discharging rates. Adding asphaltenes to paraffin has been found to increase its thermal conductivity, thus enhancing the practical prospects of these materials.^{15,16} Chemical modification of asphaltenes has also been shown to affect their aggregation behavior and control the thermal conductivity of the systems.^{14–16} Moreover, it has been established that the sedimentation stability of paraffin-based blends filled with asphaltenes can be improved using polymer compatibilizers such as poly(3-hexylthiophene).¹⁷

Most previous studies considered asphaltenes of the so-called “island” type, whose cores chemically resembled small “flakes” of graphene.¹⁸ At the same time, “island”-type asphaltenes can also be classified as discotic liquid crystalline molecules due to the presence of polycyclic aromatic cores in their composition.¹⁹ It is well known that these molecules tend to aggregate into ordered columnar rod-like stacks.¹⁹ Their aggregation is driven by π – π interactions, and these interactions can

^a Department of Physics and Astronomy, The University of Western Ontario,
1151 Richmond Street, London, Ontario, N6A 3K7, Canada

^b Institute of Macromolecular Compounds, Russian Academy of Sciences,
Bolshoj Prospect V.O. 31, St. Petersburg, 199004, Russia.
E-mail: sergey.v.lyulin@gmail.com

† Electronic supplementary information (ESI) available. See DOI: <https://doi.org/10.1039/d3cp02953k>

enable efficient heat transfer from one molecule to another in the system.^{20,21} Therefore, increasing the size of the polycyclic core can promote the self-assembly of asphaltenes into columnar aggregates and enhance the thermal conductivity of paraffin-asphaltene systems.

There are several experimental methods for modifying the size of asphaltene polycyclic cores.^{22,23} One of the simplest approaches is solvent fractionation. Based on their solubility in various solvents, asphaltenes can be separated from crude oil into fractions with different polycyclic core sizes.^{23,24} Asphaltene samples can also be subjected to pyrolysis at high temperatures to change the core sizes due to polymerization/depolymerization reactions.²⁵ In addition, Gorbacheva *et al.*¹⁶ have shown that the pyrolysis of hydrocarbon feedstock can yield so-called “technogenic” asphaltenes with high condensation and an almost complete absence of heteroatoms in polycyclic cores. Despite the availability of these methods, the precise control of the chemical structure of asphaltene molecules and the size of their cores remains an excessively complex experimental task. As a result, the effect of core sizes on the properties of asphaltene-containing systems remains largely unknown.

To fill this gap, our work focuses on the impact of the sizes of asphaltene cores on the structure and thermal properties of paraffin-based systems filled with asphaltenes. For this purpose, we performed molecular dynamics computer simulations with the use of atomistic models. This theoretical approach has been shown to give reliable results consistent with experiments for paraffin-asphaltene systems.¹⁷ At the same time, unlike experiments the simulations allow us to consider asphaltene molecules of well-defined chemical structures and understand how a subtle difference in cores may affect the asphaltene behavior and system properties in real systems.

Methods

Atomistic molecular dynamics simulations of paraffin-based systems filled with asphaltenes were carried out. To model paraffin, we used *n*-eicosane (C₂₀H₄₂, Fig. 1a) due to its potential for use in domestic thermal energy storage.²⁶ Three different model asphaltene molecules were considered, see Fig. 1. In our previous work,¹⁴ we studied the model asphaltene molecule composed of 7 aromatic rings, 1 sulfur atom, and several aliphatic groups, see Fig. 1b. We refer to this model as ASP1. According to Mullins¹ and Li and Greenfield,²⁷ the ASP1 structure is typical for asphaltenes. In this paper, we used this molecule for our comparative analysis and for building a new asphaltene model ASP2, see Fig. 1c. Namely, the ASP1 core was modified by the deletion of the sulfur-containing cycle and by transforming two rings to an aromatic form. The resulting polycyclic core of an ASP2 asphaltene can be viewed as small pyrene and phenanthrene fragments fused together. Therefore, considering this molecule would allow us to better understand the effect of core shape on the paraffin-asphaltene system's properties. It is noteworthy that the ASP2 molecule resembles the structure of so-called “technogenic” asphaltenes isolated from ethylene tar samples in ref. 16 and 28. The aliphatic periphery of this molecule consists of several methyl and ethyl groups, so that the ASP2 molecular weight amounts to about 500 g mol⁻¹ in accordance with a peak molecular weight value observed through the matrix assisted laser desorption/ionization (MALDI) spectroscopy for the most probable “technogenic” asphaltene molecules considered in ref. 16. To study how increasing the core size affects the properties of paraffin-based systems filled with asphaltenes, we considered the model asphaltene molecule ASP3 with an enlarged core, which was proposed in ref. 29, see Fig. 1d. The ASP3 core comprises 23

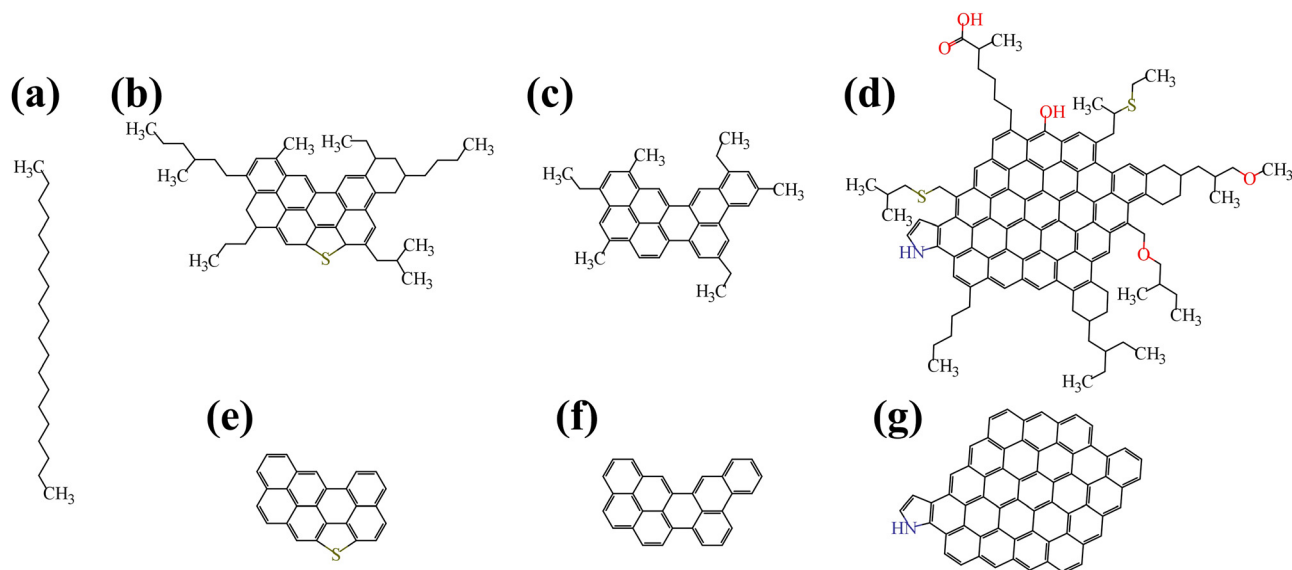


Fig. 1 The chemical structures of the constituents of the considered paraffin-asphaltene systems: (a) *n*-eicosane, (b) the ASP1 model with a typical chemical structure for asphaltenes,^{1,27} (c) the ASP2 model with a core representing fused pyrene and phenanthrene fragments, (d) the ASP3 model with an enlarged core,²⁹ and (e)–(g) the corresponding models of modified asphaltenes ASP1-M, ASP2-M, and ASP3-M with peripheral alkane groups cut off.

aromatic rings, which is about three times larger than that in the ASP1 and ASP2 molecules. Notably, the ASP3 molecular weight ($\sim 1600 \text{ g mol}^{-1}$) agrees well with a peak value in the MALDI spectra for asphaltenes isolated from crude oil of the Ashalchinskoye field.¹⁶ Since our previous study¹⁴ has shown that chemically modified asphaltenes with the aliphatic periphery cut off gave a larger increase in thermal conductivity compared to pristine asphaltenes, the modified molecules of the three model asphaltenes without aliphatic side chains (ASP1-M, ASP2-M, and ASP3-M, see Fig. 1e–g) were considered in this work for the sake of completeness.

The composition of paraffin-based systems and simulation protocol are chosen to allow comparison with the results of our previous work,¹⁴ where the ASP1 molecules were studied. Details of all systems used in our study are listed in Table 1. All systems were composed of 500 paraffin molecules and a number of asphaltene molecules, N_{asp} , depending on the type of asphaltenes. Based on ASP1-M-containing systems, we fixed the weight concentrations of fillers and chose the N_{asp} -values in our systems, see Table 1. The number of filler molecules was consistent across systems containing pristine and modified asphaltenes to preserve the molar concentration of polycyclic cores. Thus, N_{asp} was equal to 44, 99, or 214 for the ASP1 and ASP1-M molecules. In the case of ASP2 and ASP2-M asphaltenes, the system consisted of 214 filler molecules. Our focus is on a single, relatively high filler concentration because, as we proceed to show, this type of molecule demonstrates a limited ability to increase the thermal conductivity of paraffin. For the ASP3 and ASP3-M molecules, we considered several filler molecules N_{asp} equal to 21, 44, or 88. In this case, the N_{asp} -values are lower due to the enlarged sizes of these molecules compared to their counterparts, but the weight concentrations are comparable, see Table 1.

To generate the starting configurations of the systems, paraffin and asphaltene molecules were evenly distributed across the cubic simulation box with sizes of about 15 nm. Three-dimensional periodic boundary conditions were applied.³⁰

Table 1 Parameters of the simulated systems. Here N_{par} is the number of paraffin molecules, N_{asp} is the number of asphaltene molecules, C_{asp} is the weight concentration of asphaltenes, C_{core} is the weight concentration of asphaltene cores, L is the size of a simulation box edge, and N_{atoms} is the total number of atoms

System	N_{par}	N_{asp}	C_{asp} , wt%	C_{core} , wt%	L , nm	N_{atoms}
PAR-ASP1-44	500	44	18	8.8	7.4	36 016
PAR-ASP1-99	500	99	33.1	16.1	7.8	42 286
PAR-ASP1-214	500	214	51.7	25.1	8.5	55 396
PAR-ASP2-214	500	214	43.2	31.0	8.1	46 622
PAR-ASP3-21	500	21	19.2	9.4	7.4	35 788
PAR-ASP3-44	500	44	33.3	16.3	7.7	41 032
PAR-ASP3-88	500	88	49.9	24.4	8.3	51 064
PAR-ASP1-M-44	500	44	10	9.7	7.2	32 716
PAR-ASP1-M-99	500	99	20	19.3	7.4	34 861
PAR-ASP1-M-214	500	214	35	33.9	7.7	39 346
PAR-ASP2-M-214	500	214	36.3	34.7	7.7	40 844
PAR-ASP3-M-21	500	21	10.6	10.4	7.2	32 806
PAR-ASP3-M-44	500	44	20	19.5	7.3	34 784
PAR-ASP3-M-88	500	88	33.4	33.5	7.6	38 568

We then minimized the energy of each system using the steepest descent algorithm.³⁰ Next, isotropic compression was performed for 10 ns at a pressure of 50 bar and a temperature of 450 K. The time step was set to 2 fs.³⁰ The pressure and temperature were maintained using the Berendsen barostat and thermostat³¹ with the same coupling constant of 1 ps. After the compression step, the Nosé–Hoover thermostat^{32,33} with a coupling constant of 1 ps and the Parrinello–Rahman barostat³⁴ with a coupling constant of 5 ps were applied, and we ran simulations at 1 bar and 450 K. The chosen temperature enables studying the paraffin-based systems in the liquid state and reduces the simulation times required for equilibration. Simulation data for ASP1 or ASP1-M systems were taken from ref. 14. In the case of ASP2 and ASP2-M molecules, systems were run for 600 ns. Most systems filled with ASP3 or ASP3-M asphaltenes were simulated for 1 μs , except for the PAR-ASP3-44 and PAR-ASP3-88 systems, which were run for 2.5 μs and 3.3 μs , respectively. These simulation times were needed to ensure proper equilibration. For the PAR-ASP2 and PAR-ASP2-M systems, equilibration took about 100 ns of simulations. Most PAR-ASP3 and PAR-ASP3-M systems reached their equilibria during the first 0.5 μs of simulations. However, for the PAR-ASP3-44 and PAR-ASP3-88 systems, the equilibration took 0.9 μs and 2.3 μs , respectively. The equilibration times were evaluated from the time dependence of the average sizes of asphaltene aggregates in the systems, see Fig. S1 and S2 in the ESI.† Configurations of equilibrated systems were utilized to evaluate their thermal conductivity.

The thermal conductivity κ was computed from the heat flux using the Green–Kubo relation.^{35,36} In its standard form the Green–Kubo method does not account for partial enthalpy terms that might be important when multicomponent heterogeneous systems are considered. However, the corresponding correction to the thermal conductivity was shown to be relatively small for liquid and solid systems.³⁷ Because of that, the standard Green–Kubo method is often used for multicomponent composite systems.^{38–41} In practice, to evaluate the thermal conductivity, we followed closely the Green–Kubo approach employed and validated in our previous papers.^{14,17,42}

Since asphaltene molecules could form elongated stacks of arbitrary orientation in the simulation box, care has to be taken to properly account for the anisotropic contribution to the thermal conductivity κ . Within the Green–Kubo method, we first compute the per-atom stress tensor using the LAMMPS procedure centroid/stress/atom.⁴³ In general, this tensor has nine non-zero components, so such an approach is applicable to anisotropic systems. Based on the per-atom stress tensor, the heat flux vector and the thermal conductivity tensor of anisotropic paraffin–asphaltene systems are then computed. Due to anisotropy, three diagonal components of the thermal conductivity tensor differ,⁴⁴ as seen in Table S1 (ESI†). Because experiments normally provide a single value for thermal conductivity,^{15–17} in addition to κ_{xx} , κ_{yy} , and κ_{zz} we also presented our results as an average over the values of the diagonal components $\langle \kappa \rangle$, see Table S1 (ESI†).

The heat flux was calculated from 1 ns-long NVE simulations and saved every 1 fs. The autocorrelation functions of heat flux

(HFACF) were calculated with the use of the correlation time of 10 ps.⁴³ This correlation time was shown to be sufficiently long for HFACFs and their running integrals to converge, see Fig. S3 and S4 (ESI†). For computing the HFACFs, we used a modified formula for the virial, which properly accounts for the contributions of the valent angles and dihedrals.^{43,45} The calculated HFACFs were used for evaluating the thermal conductivity; the outcome of the last 500 ps was taken for averaging, see Fig. S5 (ESI†).

Equilibrated configurations of the systems were cooled down to a temperature of 250 K with a cooling rate of 6×10^9 K min⁻¹. This cooling rate required a 10 K step change in temperature every 100 ns, amounting to 21 steps or 2.1 μ s of simulation time for each cooling-rate simulation. While computationally demanding, a cooling rate of this magnitude has been previously demonstrated as being necessary to accurately model the temperature-dependent changes in mass density and thermal conductivity that occur in paraffin during crystallization.⁴⁶

All simulations were performed using the all-atom CHARMM36 force field.^{47,48} The aggregation of asphaltenes stems from π - π interactions. The performance of a point charge all-atom model in the description of these interactions, based on a proper force field such as CHARMM36, is determined by both Lennard-Jones and Coulomb potentials.⁴⁹ Our previous study¹⁴ found that the CHARMM36 parameter set successfully describes π - π interactions. Moreover, for modified asphaltenes without peripheral alkane groups, this force field reproduced extended columnar aggregates typical for discotic liquid crystalline molecules, *e.g.*, coronene.⁵⁰ At the same time, CHARMM36 was also shown to produce reliable results for the properties of *n*-eicosane.^{51,52} All these justified the use of the CHARMM36 force field for computer simulations of paraffin-asphaltene systems. A 1.2 nm cut-off radius was set for the non-bonded interactions. A switch function between 1.0 and 1.2 nm was applied to treat the van der Waals interactions.^{47,48} The bonds involving hydrogen atoms were constrained with the P-LINCS algorithm.^{30,53} The long-range electrostatic interactions were calculated with the particle-mesh Ewald method.⁵⁴

The analysis of thermal conductivity was carried out with the LAMMPS package,⁵⁵ while molecular dynamics simulations were performed using the GROMACS package.⁵⁶ The force field parameters were generated with the CHARMM-GUI web server.^{57,58} The InterMol software was employed to convert the force field files from GROMACS to LAMMPS format.⁵⁹ The VMD suite was used to prepare all the snapshots.⁶⁰

Results

1. Asphaltene molecules with small cores

To understand the role of the size of asphaltene cores in determining the properties of paraffin-asphaltene systems, we first focus on the asphaltenes with relatively small cores and compare the paraffin systems filled with ASP2 and ASP1 asphaltenes. In particular, we analyzed radial distribution functions

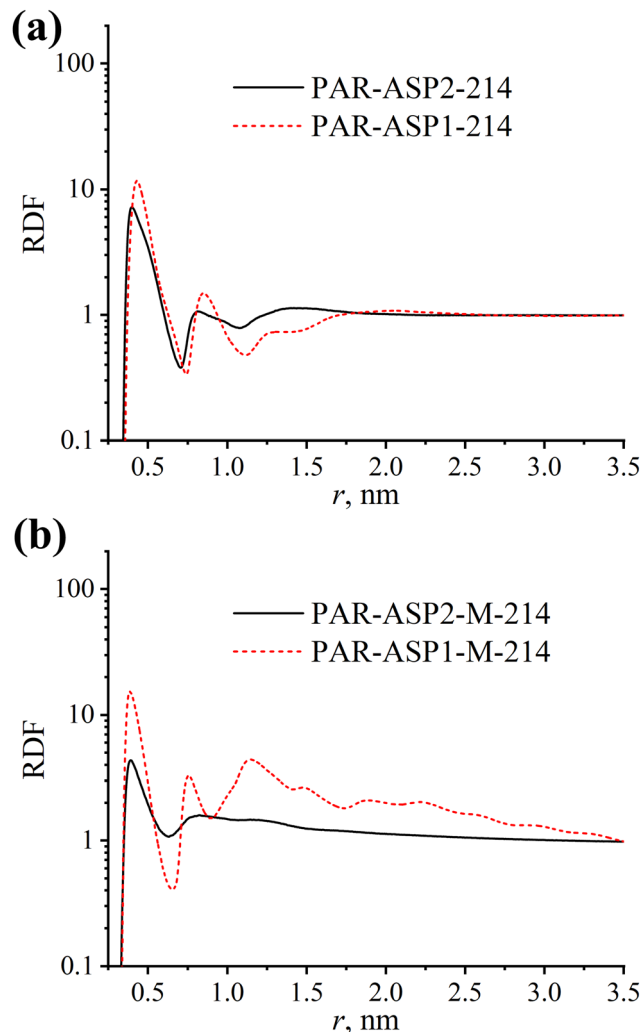


Fig. 2 The radial distribution functions (RDF) for the centers of mass of polycyclic cores of pristine (a) and modified (b) ASP2 and ASP1 asphaltenes in liquid paraffin-asphaltene systems.

(RDFs) for the centers of mass of polycyclic asphaltene cores in liquid paraffin-asphaltene systems, see Fig. 2. Physically, the RDF qualitatively describes the probability of finding one asphaltene core at a distance r from another core in the system. Therefore, it allows us to shed light on the aggregation behavior of the asphaltenes and the strength of interactions between considered molecules.

Fig. 2a shows that at the largest considered filler concentration, both ASP2 and ASP1 asphaltenes form small aggregates in paraffin. A well-defined main RDF peak at $r \sim 0.4$ nm and a subsequent second peak at $r \sim 0.8$ nm correspond to the distances between adjacent molecules and molecules separated by one asphaltene within the aggregates, respectively. It can be seen that the RDF curve for ASP2 asphaltenes at $r \sim 1.4$ nm is located above 1 in contrast to that for ASP1 asphaltenes, *i.e.*, ASP2 asphaltenes form aggregates slightly larger than ASP1 asphaltenes. This difference can be explained by the fact that the ASP2 molecules have smaller aliphatic side groups responsible for mixing asphaltenes with paraffin. More importantly, the first two

RDF peaks for ASP1 asphaltenes are slightly higher compared to those for ASP2 asphaltenes, see Fig. 2a. This indicates that ASP1 molecules interact stronger than their ASP2 counterparts.

If the alkane side groups of the asphaltene molecules are cut off, the tendency of asphaltenes to aggregate increases, see Fig. 2b. As it follows from the RDF-values above 1 at $r > 0.7$ nm, ASP1-M and ASP2-M molecules form large aggregates. For ASP1-M molecules, the RDF curve has a complex shape with multiple maxima. This was previously shown to be due to the self-assembly of these asphaltenes into a bundle of interacting columnar stacks involving almost all of the filler molecules in the system.¹⁴ In contrast, only a single prominent peak at $r \sim 0.4$ nm corresponding to adjacent stacked molecules is seen in the RDF dependence for ASP2-M molecules, see Fig. 2b. Then, the RDF gradually decreases to 1. Thus, ASP2-M asphaltenes do not form extended columns, but their dimers randomly assemble with each other into a disordered structure. It is important to emphasize that both the shape of the RDF and the height of its peaks clearly show that the interaction of ASP2-M asphaltenes is much weaker than ASP1-M asphaltenes.

The insight gained from the RDF curves was confirmed by a visual analysis of the system snapshots. Fig. 3a shows that the ASP2 molecules are almost uniformly distributed throughout the simulation box similar to the ASP1 molecules (Fig. 3c), whereas large, disordered aggregates or columnar structures can be formed in the case of the ASP2-M or ASP1-M molecules, respectively, see Fig. 3b and d.

In addition to structural properties, the thermal conductivity of systems filled with ASP2 or ASP2-M asphaltenes was evaluated. Previous simulation studies have shown that the coefficient of the thermal conductivity κ of pure liquid *n*-eicosane at

$T = 450$ K equals 0.197 ± 0.002 W (m K)⁻¹.⁴² It turns out that the addition of ASP2 asphaltenes to the paraffin system increases the κ -value to 0.21 ± 0.01 W (m K)⁻¹, which is 7% larger than that for unfilled paraffin. A similar increase in the κ -value was previously reported for ASP1 asphaltenes.¹⁴ As far as the ASP2-M molecules are concerned, they increased the κ -value to 0.24 ± 0.01 W (m K)⁻¹, *i.e.*, by about 22%. In turn, the use of ASP1-M asphaltenes as a filler yielded $\kappa = 0.71 \pm 0.01$ W (m K)⁻¹.¹⁴ Thus, the less ordered structure of ASP2 and ASP2-M aggregates resulted in their poorer performance as thermal conductivity enhancers compared to the ASP1-M model.

2. Asphaltenes with enlarged cores: the structure of paraffin-asphaltene systems

As is clearly seen from the previous section, the aggregation behavior of asphaltenes with small cores can be greatly affected by a subtle difference in the shape of the aromatic cores. While the cores of ASP1 and ASP2 asphaltenes have comparable sizes, the shapes of their cores differ. ASP1 asphaltenes are characterized by a compact core, whereas the core of the ASP2 molecules is more extended and asymmetric, see Fig. 1. As we showed above, such an asymmetry impairs the ability of ASP2 asphaltenes to form extended ordered aggregates and, correspondingly, to enhance the thermal conductivity of paraffin-asphaltene systems. A primary focus of our study is the impact of the size of an asphaltene core on the properties of a paraffin-asphaltene mixture. Given the limitations inherent to atomistic computer simulations, an enlarged core has to be chosen in such a way that it would allow one to observe noticeable changes in the aggregation behavior on spatial and time scales accessible for simulations. To achieve this, one should avoid extended, asymmetric cores, as is shown in the previous section. Therefore, a molecule with a rather compact aromatic core was chosen as a model for asphaltenes with enlarged cores, see the asphaltene ASP3 in Fig. 1d. In the following, we will compare the properties of paraffin systems with ASP3 and ASP1, thereby focusing on the effect of the size of the core (and not their shape).

In Fig. 4a–c we present the RDFs for the centers of mass of ASP1 and ASP3 asphaltenes in liquid paraffin-asphaltene systems at different filler concentrations. It is clearly seen that the first RDF peak at $r \sim 0.4$ nm originating from two stacked asphaltene molecules is much higher for ASP3 molecules than for their ASP1 counterparts. Thus, the enlarged core does lead to stronger π - π interactions. One can also notice that the RDF curves for the ASP3 molecule in Fig. 4a–c are characterized by a larger number of peaks compared to those for the ASP1 model. Based on the number of peaks, ASP1 asphaltenes mainly aggregate into dimers and trimers, whereas ASP3 molecules can form extended columns involving more than six molecules. As their RDF-values approach 1 at large distances ($r > 1$ nm), ASP1 molecules are uniformly distributed in the system, regardless of the filler concentration. In the PAR-ASP3-21 system, multiple peaks whose height decreases with r indicate the formation of a long columnar aggregate, see Fig. 4a. Increasing the number of filler molecules from 21 to 44 and 88 leads to the

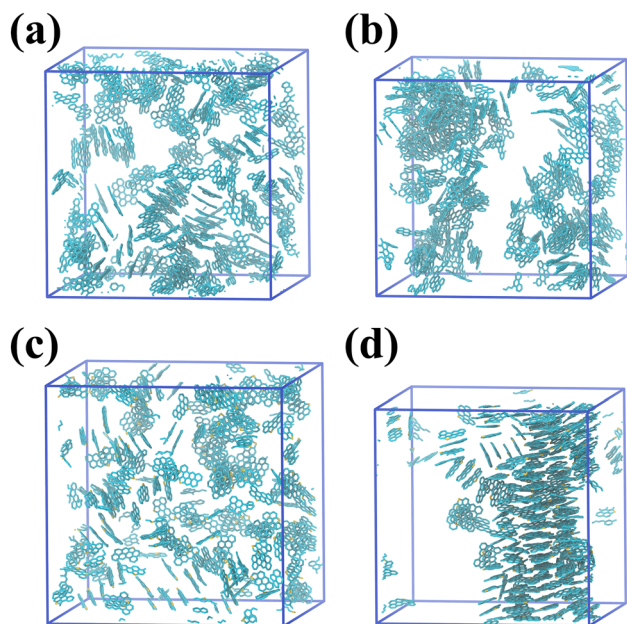


Fig. 3 Representative snapshots of asphaltene cores in (a) PAR-ASP2-214, (b) PAR-ASP2-M-214 systems, (c) PAR-ASP1-214, and (d) PAR-ASP1-M-214.

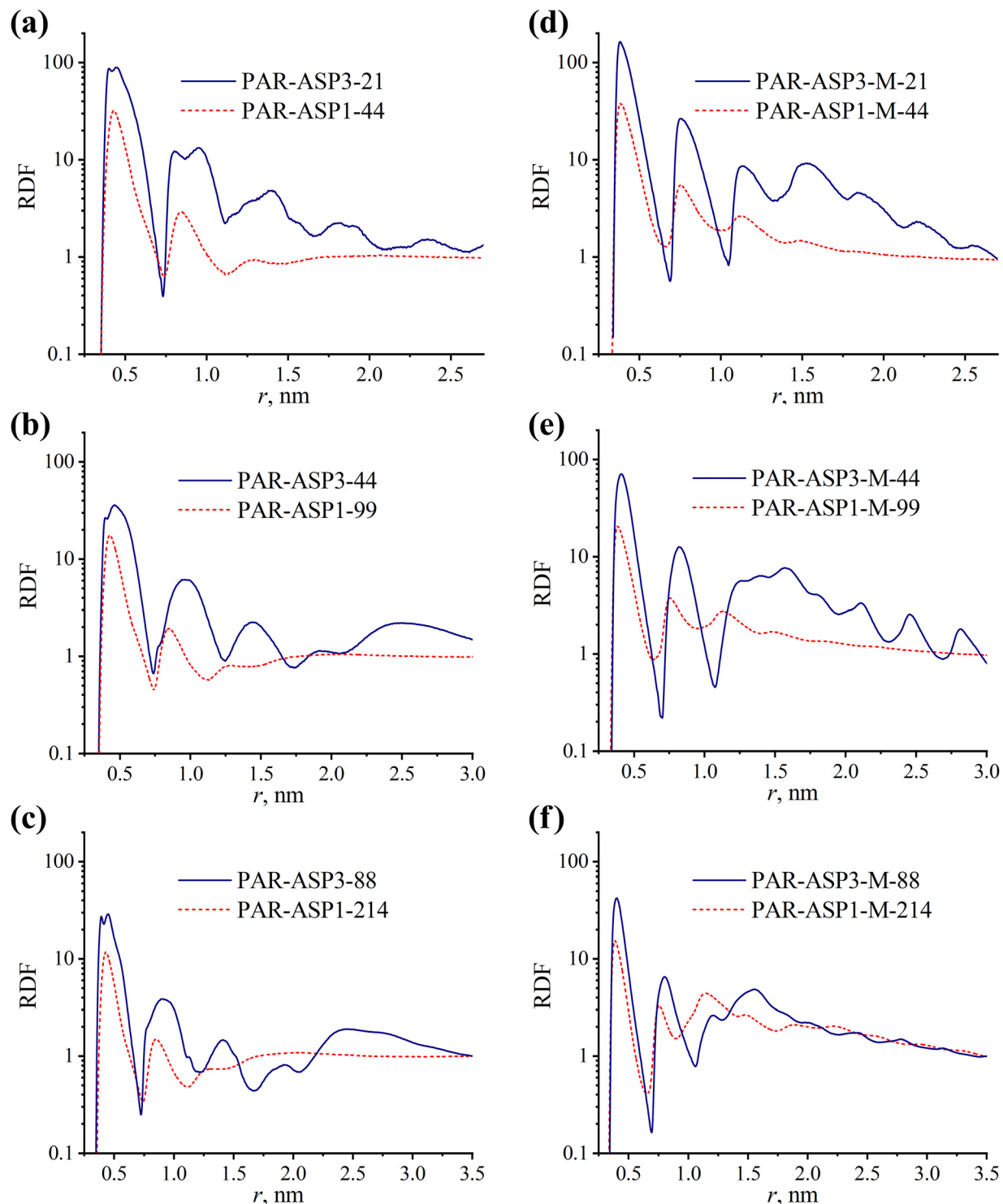


Fig. 4 The radial distribution functions (RDF) for the centers of mass of polycyclic cores of pristine (a)–(c) and modified (d)–(f) ASP3 and ASP1 asphaltenes in liquid paraffin–asphaltene systems at various filler concentrations. Each figure shows RDF at the same weight concentration for asphaltenes of different sizes.

emergence of a broad peak at $r \sim 2.5$ nm with RDF-values above 1. This probably means that asphaltene columns interact with each other at these filler concentrations.

The interaction and aggregation of modified ASP3-M molecules with each other are stronger than both pristine ASP3 and

modified ASP1-M molecules at all considered filler concentrations, see Fig. 4d–f. Again, multiple peaks indicate the formation of columnar structures. Due to the enlarged core, ASP3-M molecules form longer columns than ASP1-M molecules at a given filler concentration. Moreover, high RDF-values at $r > 1$ nm

suggest that ASP3-M molecules self-assemble into bundles of several interacting columns, irrespective of the filler concentration. This is in contrast with PAR-ASP3 systems, where the columns dissolve in paraffin, possibly due to the presence of aliphatic side chains in the asphaltene composition. In the case of ASP1-M asphaltenes, the bundles are observed only at the largest filler concentrations considered (the PAR-ASP1-M-214 system), see Fig. 4f.

Visual inspection of the asphaltene distributions in the systems confirms the conclusions made from RDFs, see Fig. 5. In particular, several columns are observed in most systems, with the exception of the PAR-ASP3-21 system, where only one column is present. The column length of both ASP3 and ASP3-M molecules increases with the number of asphaltenes in the system. It is important to emphasize that ASP3 molecules are able to form extended structures, which is not the case for ASP1 asphaltenes (Fig. 4). Due to the large size of the aromatic cores, the presence of steric interactions between the aliphatic side groups of ASP3 molecules does not prevent the formation of extended stacks or columns. It is also seen that ASP3 asphaltenes form single-column structures, while ASP3-M molecules can be surrounded by other asphaltenes in bundles. Notably, ASP3 columns themselves and ASP3-M columns in bundles can be oriented in a complex manner.

To get further insight into the aggregation behavior of asphaltenes, we focus on the average size of the asphaltene aggregates, N_{av} , as well as on their orientational order parameter S calculated for vectors normal to the asphaltene cores

(see Fig. S6 in the ESI† for details) in analogy to ref. 61. The results are presented in Table 2. It turns out that ASP1 molecules form relatively small aggregates, whose size slightly increases with filler concentration. At the lowest considered filler concentration of 21 molecules, ASP3 asphaltenes form an aggregate that includes all the filler in the system. An increase in the number of ASP3 asphaltenes leads to an increase in aggregate size, and N_{av} -values indicate the presence of several aggregates. Meanwhile, the ordering of ASP3 and ASP1 asphaltenes varies in a similar fashion, it decreases with asphaltene concentration.

Notably, the molecular ordering is much higher for ASP3 asphaltenes than for ASP1 molecules, see Table 2.

As for modified asphaltenes, the aggregate size N_{av} increases with filler concentration for both ASP3-M and ASP1-M asphaltenes, with the former molecules self-assembling into a single aggregate consisting of all the filler molecules in the system. For ASP1-M molecules, the order parameter S remains almost constant for 44 and 99 asphaltenes in the system and then increases with the filler concentration. ASP3-M asphaltenes, however, exhibit an opposite trend in the change of their ordering. Namely, increasing the number of filler molecules from 21 to 88 first does not change the S -value of about 0.9–1 and then drops it to about 0.6; this drop occurs since bundles orient in different directions at the high filler concentration, see Fig. 5d–f. Overall, the concentration of asphaltene cores is a key parameter that determines the aggregation and ordering of the filler. Meanwhile, increasing the core size not only

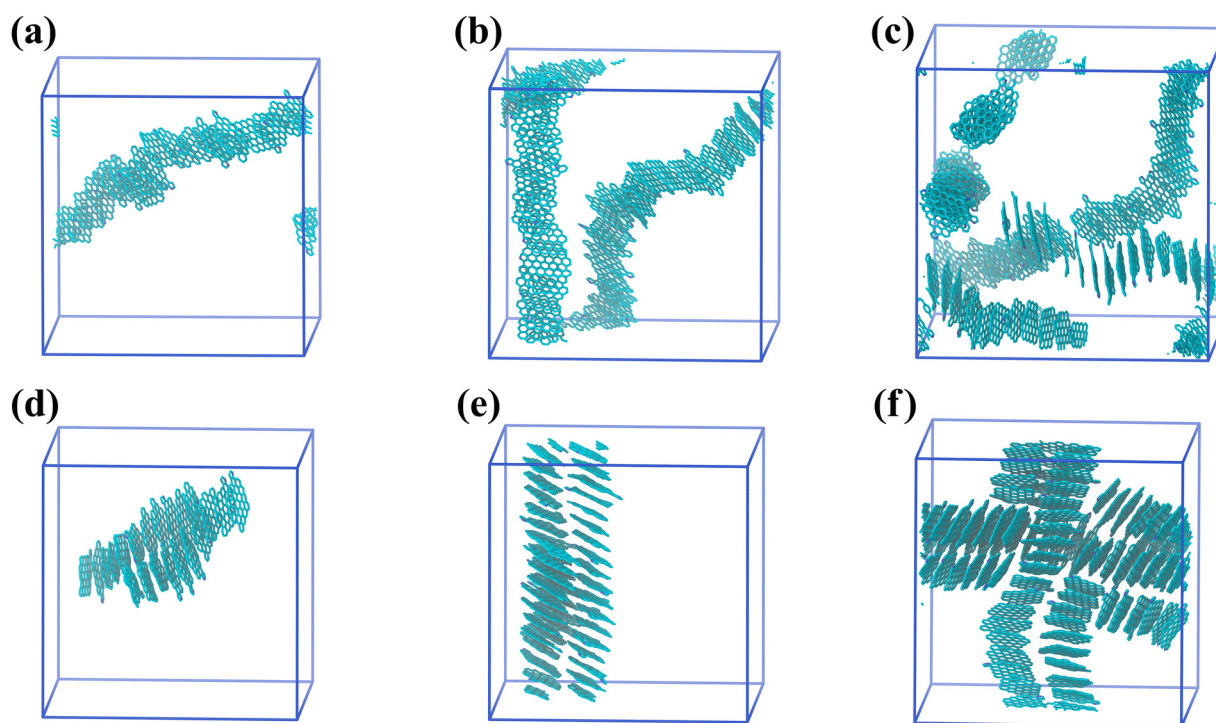


Fig. 5 Representative snapshots of asphaltene cores in (a) PAR-ASP3-21, (b) PAR-ASP3-44, (c) PAR-ASP3-88, (d) PAR-ASP3-M-21, (e) PAR-ASP3-M-44, and (f) PAR-ASP3-M-88 systems.

Table 2 Average sizes of asphaltene aggregates N_{av} , the orientational order parameter of asphaltenes S calculated for vectors normal to the asphaltene cores, and the crystallization temperature T_c

System	N_{av} , molecules	S	T_c , K
PAR-ASP3-21	21.0 ± 1.0	0.98 ± 0.01	310 ± 10
PAR-ASP3-44	22.5 ± 3.4	0.92 ± 0.05	290 ± 10
PAR-ASP3-88	44.0 ± 1.0	0.70 ± 0.10	295 ± 10
PAR-ASP1-44	3.1 ± 0.4	0.22 ± 0.08	310 ± 10
PAR-ASP1-99	3.6 ± 0.3	0.16 ± 0.06	310 ± 10
PAR-ASP1-214	4.8 ± 0.4	0.13 ± 0.04	—
PAR-ASP3-M-21	21.0 ± 1.0	0.92 ± 0.14	335 ± 10
PAR-ASP3-M-44	44.0 ± 1.0	0.99 ± 0.01	315 ± 10
PAR-ASP3-M-88	88.0 ± 1.0	0.58 ± 0.05	335 ± 10
PAR-ASP1-M-44	5.2 ± 1.8	0.23 ± 0.08	320 ± 10
PAR-ASP1-M-99	14.0 ± 6.5	0.22 ± 0.09	320 ± 10
PAR-ASP1-M-214	72.3 ± 25.0	0.71 ± 0.07	320 ± 10

strengthens the interactions between asphaltene molecules but also significantly enriches the aggregation behavior.

3. Asphaltenes with enlarged cores: thermal properties of paraffin-asphaltene systems

After having described the structure, we turn to the consideration of thermal properties. Our analysis is based on the temperature dependence of mass density ρ for paraffin-asphaltene systems with pristine and modified ASP3 and ASP1 molecules, see Fig. 6. It has been found that these asphaltenes affect the results in different ways.

In particular, in the high temperature domain at $T > 330$ K, the density ρ of a PAR-ASP3 system at a given filler concentration is greater than that for both pure paraffin and a PAR-ASP1 system, see Fig. 6a. This is probably due to the formation of densely packed aggregates whose density exceeds the density of paraffin and ASP1 aggregates. An increase in filler concentration leads to an increase in ρ -values as the aggregates also become larger. At temperatures around 320 K, an abrupt density increase of PAR-ASP3 systems upon cooling is observed, indicating crystallization. A temperature in the

middle of the interval of the abrupt change can be defined as the crystallization temperature T_c ,⁵¹ see Table 2. For pure paraffin, $T_c = 320$ K.⁵¹ One can also note that the magnitude of the abrupt density increase is smaller compared to pure paraffin. Meanwhile, the onset of crystallization is shifted by up to about 20 degrees towards lower temperatures than that for pure paraffin, see Fig. 6a. In other words, ASP3 asphaltenes limit the crystallization of paraffin and can slightly reduce the transition temperature, see Table 2. This effect can stem from the mixing of paraffin with asphaltene side groups. They are more extended compared to those of ASP1 asphaltenes and can therefore more strongly mix with paraffin molecules and disrupt their packing and paraffin density. As a result, the ρ -values at $T = 250$ K for the PAR-ASP3-21 and PAR-ASP3-44 systems are comparable to those of their counterparts, although they were larger at higher temperatures. ASP3 asphaltene molecules, however, do not suppress crystallization in contrast to what is witnessed in the case of ASP1 asphaltenes at high filler concentrations, see Fig. 6a.

Fig. 6b shows that the addition of ASP3-M and ASP1-M asphaltenes increases in a similar manner to the density at high temperatures corresponding to the liquid state. It can also be seen that although the presence of the ASP1-M molecules does not affect the crystallization temperature, for the PAR-ASP3-M-21 and PAR-ASP3-M-88 systems, the onset of crystallization is slightly shifted towards higher temperatures. Such a behavior is opposite to what was observed for PAR-ASP3 systems (Fig. 6a and Table 2). No such shift is seen for the PAR-ASP3-M-44 system. We note that more detailed insight into the ability of ASP3-M asphaltenes to initiate crystallization requires extensive cooling rate simulations of many independent system configurations. Such analysis, being computationally very expensive for the systems of the considered size, is beyond the scope of our paper. It should be mentioned that the magnitude of the density increase during crystallization for PAR-ASP3-M and PAR-ASP1-M systems is lower than for pure paraffin. Thus, the presence of modified

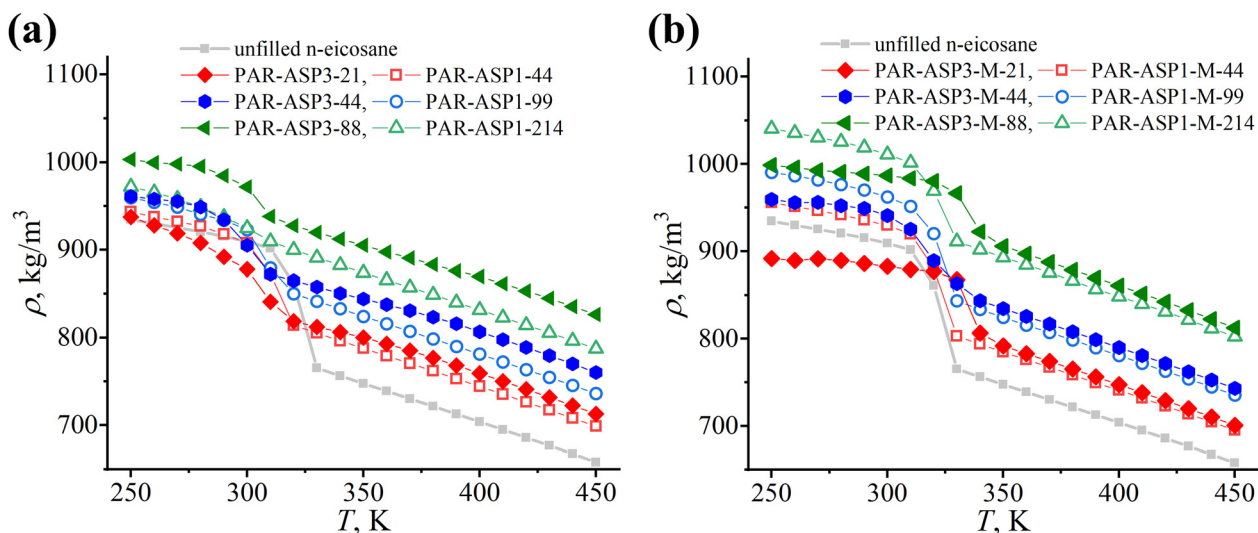


Fig. 6 Temperature dependence of density ρ for the paraffin systems filled with pristine (a) and modified (b) ASP3 and ASP1 asphaltenes.

asphaltene molecules can slightly affect system crystallization. This is a possible reason why ρ -values at low temperatures are lower for PAR-ASP3-M systems with columnar aggregates compared to paraffin. Nevertheless, crystallization is observed for both types of modified asphaltenes at all considered filler concentrations.

4. Asphaltenes with enlarged cores: thermal conductivity

Let us now proceed with an analysis of the thermal conductivity κ of the simulated systems. Our previous study¹⁴ showed that the asphaltene-induced enhancement of the thermal conductivity of paraffin systems vanished upon cooling due to a reduction in the overlap of adjacent asphaltene molecules in the aggregate and structural changes of the columnar aggregates with temperature. Therefore, here we do not consider low temperatures and focus on comparing the thermal conductivity coefficients for liquid paraffin-based systems filled with pristine and modified ASP3 and ASP1 asphaltenes at $T = 450$ K.

As mentioned in the Methods section, the formation of anisotropic asphaltene aggregates leads to a difference in the diagonal components of the thermal conductivity tensor. Indeed, as can be seen in Table S1 (ESI[†]), diagonal components κ_{xx} , κ_{yy} , and κ_{zz} differ for all considered asphaltene-paraffin systems. It is noteworthy that this difference can be linked directly to the degree of anisotropy of asphaltene aggregates. As discussed above, the formation of elongated anisotropic aggregates is promoted by the increase in the size of the asphaltene core and in the asphaltene concentration, as well as by removing the aliphatic side groups. All these factors lead to larger deviations of diagonal components from the average values, see Table S1 (ESI[†]). Overall, this deviation varies from 10% (the PAR-ASP1-99 system) to almost 50% (the PAR-ASP3-M-88 system).

To explore how asphaltene aggregation affects the thermal conductivity of a system, we considered the average values of the diagonal components of the thermal conductivity, see Fig. 7. It has to be emphasized that such an approach is an approximation for anisotropic systems and is used here solely to link our computational results with experiments, where a single value for the thermal conductivity is normally measured.^{15–17} Real systems are much larger than those considered in our simulations, so anisotropic asphaltene aggregates can be randomly oriented within a sample. This implies that a system, being anisotropic on sufficiently small scales, can be considered isotropic on larger scales, thereby justifying our approach.

As evident from Fig. 7a, both ASP3 and ASP1 molecules increase the κ -values for paraffin-asphaltene systems in comparison with pure liquid paraffin. At the lowest considered filler concentration, both asphaltenes increase thermal conductivity by $\sim 45\%$. When the asphaltene concentration reaches moderate values, the κ -value increases for the PAR-ASP3-44 system and decreases for the PAR-ASP1-99 system. The opposite change at this filler concentration can be associated with a difference in the aggregation of asphaltenes: ASP1 molecules form small, disordered aggregates, while ASP3 asphaltene aggregate into extended column-like ordered structures, see Fig. 5 and Table 2. It should be emphasized that the thermal conductivity in the case of ASP3 asphaltene exceeds that of the PAR-ASP1 system and pure paraffin by about 80% and 90%, respectively. A further increase in filler concentration does not result in a noticeable change in the κ -value for a system with ASP1 asphaltenes. However, for the PAR-ASP3-88 system a 20% decrease in thermal conductivity is observed compared to the PAR-ASP3-44 system. At the highest considered

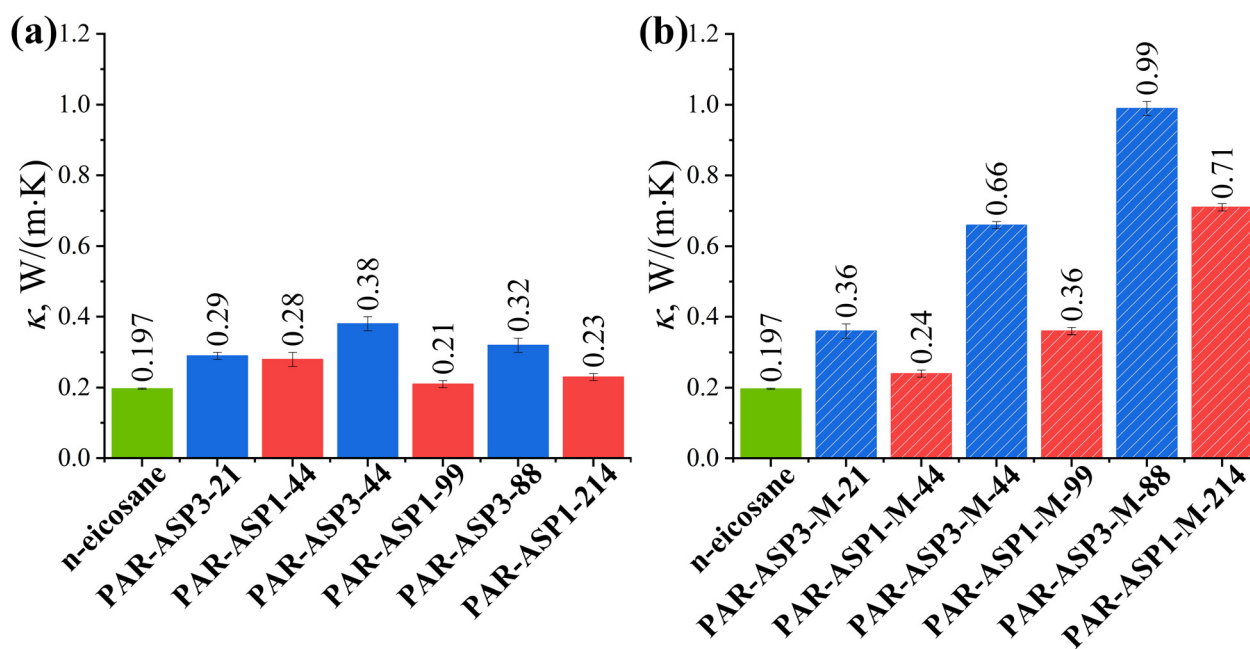


Fig. 7 Thermal conductivity coefficients κ of systems filled with pristine (a) and modified (b) ASP3 and ASP1 asphaltenes at $T = 450$ K.

filler concentration, several asphaltene columns are present in the system. The slightly different mutual orientation of these columns observed in Fig. 5 can be the reason for the lower order of asphaltenes (Table 2) and therefore for the lower κ -value compared to the PAR-ASP3-44 system. Despite this decrease, the paraffin systems filled with ASP3 molecules with an enlarged core have a larger thermal conductivity than the PAR-ASP1 systems.

Fig. 7b shows that the modified asphaltenes enhance thermal conductivity even to a greater degree than the pristine asphaltenes. The κ -values increase with filler concentration for both ASP3-M and ASP1-M molecules. At the same time, the addition of ASP3-M asphaltenes yields a greater enhancement in thermal conductivity at all considered concentrations. For instance, the κ -value for the PAR-ASP3-M-44 system exceeds that for PAR-ASP1-M-99 by about 80%. When increasing the number of ASP3-M molecules from 44 to 88, one can note an increase in the thermal conductivity for the PAR-ASP3-M-88 system despite the decrease in the asphaltene order (Table 2). This can be associated with the fact that the size of aggregates increases with the filler concentration. Thus, the thermal conductivity can be a function not only of the filler concentration, but also of the order parameter and aggregate sizes. It should be stressed that due to the formation of aggregates of complex shapes and orientations (Fig. 5), establishing a direct correlation between thermal conductivity, system composition, and asphaltene aggregation characteristics is a challenging task.

Conclusions

We have explored the effect of adding asphaltenes with polycyclic aromatic cores of different sizes on the structural and thermophysical properties of paraffin-based phase change materials. Using atomistic molecular dynamics simulations, three model asphaltene molecules (ASP1, ASP2, and ASP3) with different sizes of the core were considered: (i) the previously studied ASP1 model asphaltene with a 7-ring core typical for petroleum asphaltenes; (ii) the ASP2 model asphaltene represented a modification of the ASP1 asphaltene consisting of pyrene and phenanthrene fragments fused together; and (iii) the ASP3 model asphaltene consisting of an enlarged core of about 20 rings and several aliphatic side groups. For these model asphaltenes, we also studied the effect of their chemical modification and repeated simulations for asphaltenes with the aliphatic side groups cut off. We found that the interaction of ASP2 asphaltenes with each other is weaker than ASP1 asphaltenes, irrespective of the presence of an aliphatic periphery. This is most likely due to the asymmetric, rather than the extended shape of the aromatic cores of ASP2 asphaltenes. As a result, the ASP2 molecules are not able to form ordered structures and therefore demonstrate low efficiency as thermal conductivity enhancers of paraffins. As far as the ASP3 molecules with an enlarged core are concerned, their intermolecular interactions are found to be much stronger as compared to their counterparts with smaller cores (ASP1 and ASP2 asphaltenes).

Correspondingly, the ASP3 molecules form extended single-column aggregates in the case of pristine asphaltenes and self-assemble into bundles of several columns when the aliphatic side groups of ASP3 asphaltenes are cut off. The presence of asphaltenes with enlarged cores can slightly shift the crystallization temperature towards lower values for pristine fillers and higher temperatures for modified ones. Notably, for these asphaltenes, the liquid-crystal-line transition was observed at all filler concentrations considered, whereas the smaller molecules suppressed crystallization at high filler concentrations due to their uniform distribution and the interaction of their aliphatic side groups with paraffin molecules. Most importantly, adding the ASP3 asphaltenes with enlarged cores to the liquid paraffin results in increased thermal conductivity compared to the smaller molecules. At a concentration of aromatic cores of ~ 20 wt%, these asphaltenes, both pristine and modified ones, demonstrated an increase in thermal conductivity that was about 80% higher than that for ASP1 asphaltenes. Compared to pure liquid paraffin, the enhancement of thermal conductivity was $\sim 90\%$ for pristine ASP3 molecules and $\sim 335\%$ for modified ASP3-M asphaltenes with aliphatic side group cut off. Thus, our results clearly show that the size of asphaltene aromatic cores is one of the key parameters determining the effectiveness of asphaltenes as thermal conductivity enhancers for paraffin. From a practical perspective, the application of experimental methods, such as fractionation, is highly desirable to obtain asphaltene samples with enlarged cores and low aliphatic side chain content, as these fillers can significantly improve paraffin-based heat storage devices.

Conflicts of interest

There are no conflicts to declare.

Acknowledgements

This work was supported by the Russian Science Foundation under Agreement No. 19-13-00178 (A. A. G. and V. M. N.). The simulations were performed using the computational resources of the Institute of Macromolecular Compounds RAS, the resources of the Federal collective usage center “Complex for Simulation and Data Processing for Mega-Science Facilities” at NRC “Kurchatov Institute” (<https://ckp.nrcki.ru/>), and the equipment of the shared research facilities of HPC computing resources at the Lomonosov Moscow State University.

References

- 1 O. C. Mullins, *Annu. Rev. Anal. Chem.*, 2011, **4**, 393–418.
- 2 K. Akbarzadeh, H. Alboudwarej, W. Y. Svrcek and H. W. Yarranton, *Fluid Phase Equilib.*, 2005, **232**, 159–170.
- 3 L. V. Meléndez, A. Lache, J. A. Orrego-Ruiz, Z. Pachón and E. Mejía-Ospino, *J. Pet. Sci. Eng.*, 2012, **90–91**, 56–60.
- 4 S. O. Ilyin, M. P. Arinina, M. Y. Polyakova, V. G. Kulichikhin and A. Y. Malkin, *Fuel*, 2016, **186**, 157–167.
- 5 The IEA Oil Market Report, 2023, <https://www.iea.org/topics/oil-market-report>.

- 6 A. Ghassemirad, N. Bala, L. Hashemian and A. Bayat, *Constr. Build. Mater.*, 2021, **290**, 123200.
- 7 H. Wu, V. K. Thakur and M. R. Kessler, *J. Mater. Sci.*, 2016, **51**, 2394–2403.
- 8 M. N. Siddiqui, *Polym. Compos.*, 2017, **38**, 1957–1963.
- 9 V. Y. Ignatenko, S. V. Antonov, A. V. Kostyuk, N. M. Smirnova, V. V. Makarova and S. O. Ilyin, *Russ. J. Appl. Chem.*, 2019, **92**, 1712–1717.
- 10 R. E. Abujnah, H. Sharif, B. Torres, K. Castillo, V. Gupta and R. R. Chianelli, *J. Environ. Anal. Toxicol.*, 2016, **6**, 1000345.
- 11 U. K. Bhui, A. Ray and M. P. Joshi, *Macromolecular Characterization of Hydrocarbons for Sustainable Future*, Springer, Singapore, 2021, pp. 129–139.
- 12 N. I. Borzdun, R. R. Ramazanov, A. D. Glova, S. V. Larin and S. V. Lyulin, *Energy Fuels*, 2021, **35**, 8423–8429.
- 13 N. Borzdun, A. Glova, S. Larin and S. Lyulin, *Nanomaterials*, 2022, **12**, 2867.
- 14 A. D. Glova, V. M. Nazarychev, S. V. Larin, A. V. Lyulin, S. V. Lyulin and A. A. Gurtovenko, *J. Mol. Liq.*, 2022, **346**, 117112.
- 15 V. V. Makarova, S. N. Gorbacheva, A. V. Kostyuk, S. V. Antonov, Y. Y. Borisova, D. N. Borisov and M. R. Yakubov, *J. Energy Storage*, 2022, **47**, 103595.
- 16 S. N. Gorbacheva, Y. Y. Borisova, V. V. Makarova, S. V. Antonov, D. N. Borisov and M. R. Yakubov, *Molecules*, 2023, **28**, 949.
- 17 S. V. Larin, V. V. Makarova, S. N. Gorbacheva, M. R. Yakubov, S. V. Antonov, N. I. Borzdun, A. D. Glova, V. M. Nazarychev, A. A. Gurtovenko and S. V. Lyulin, *J. Chem. Phys.*, 2022, **157**, 194702.
- 18 M. W. Boomstra, M. W. J. van Asseldonk, B. J. Geurts, V. M. Nazarychev and A. V. Lyulin, *Int. J. Heat Mass Transfer*, 2022, **195**, 123192.
- 19 T. Wöhrle, I. Wurzbach, J. Kirres, A. Kostidou, N. Kapernaum, J. Litterscheidt, J. C. Haenle, P. Staffeld, A. Baro, F. Giesselmann and S. Laschat, *Chem. Rev.*, 2016, **116**, 1139–1241.
- 20 G. Kiršanskas, Q. Li, K. Flensberg, G. C. Solomon and M. Leijnse, *Appl. Phys. Lett.*, 2014, **105**, 233102.
- 21 M. Park, D.-G. Kang, H. Ko, M. Rim, D. T. Tran, S. Park, M. Kang, T.-W. Kim, N. Kim and K.-U. Jeong, *Mater. Horiz.*, 2020, **7**, 2635–2642.
- 22 P. Zuo, S. Qu and W. Shen, *J. Energy Chem.*, 2019, **34**, 186–207.
- 23 L. I. Musin, L. E. Foss, K. V. Shabalin, O. A. Nagornova, Y. Y. Borisova, D. N. Borisov and M. R. Yakubov, *Energy Fuels*, 2020, **34**, 6523–6543.
- 24 Y. Y. Borisova, L. I. Musin, D. N. Borisov and M. R. Yakubov, *Pet. Chem.*, 2021, **61**, 424–430.
- 25 S. Akmaz, M. A. Gurkaynak and M. Yasar, *J. Anal. Appl. Pyrolysis*, 2012, **96**, 139–145.
- 26 A. Sharma, V. V. Tyagi, C. R. Chen and D. Buddhi, *Renewable Sustainable Energy Rev.*, 2009, **13**, 318–345.
- 27 D. D. Li and M. L. Greenfield, *Fuel*, 2014, **115**, 347–356.
- 28 C. Ge, Z. Sun, H. Yang, D. Long, W. Qiao and L. Ling, *New Carbon Mater.*, 2018, **33**, 71–81.
- 29 E. Rogel, *Energy Fuels*, 2000, **14**, 566–574.
- 30 M. Abraham, B. Hess, D. Van der Spoel and E. Lindahl, *Gromacs user manual version 5.1.4*, Royal Institute of Technology and Uppsala University, Sweden, 2016.
- 31 H. J. C. Berendsen, J. P. M. Postma, W. F. van Gunsteren, A. DiNola and J. R. Haak, *J. Chem. Phys.*, 1984, **81**, 3684–3690.
- 32 S. Nosé, *Mol. Phys.*, 1984, **52**, 255–268.
- 33 W. G. Hoover, *Phys. Rev. A: At., Mol., Opt. Phys.*, 1985, **31**, 1695–1697.
- 34 M. Parrinello and A. Rahman, *J. Appl. Phys.*, 1981, **52**, 7182–7190.
- 35 M. S. Green, *J. Chem. Phys.*, 1954, **22**, 398–413.
- 36 R. Kubo, *J. Phys. Soc. Jpn.*, 1957, **12**, 570–586.
- 37 H. Babaei, P. Keblinski and J. M. Khodadadi, *J. Appl. Phys.*, 2012, **112**, 054310.
- 38 N. A. Fasanella and V. Sundararaghavan, *JOM*, 2016, **68**, 1396–1410.
- 39 B. Mortazavi, F. Hassouna, A. Laachachi, A. Rajabpour, S. Ahzi, D. Chapron, V. Toniazzo and D. Ruch, *Thermochim. Acta*, 2013, **552**, 106–113.
- 40 Z. Liu, J. Li, C. Zhou and W. Zhu, *J. Heat Mass Transfer*, 2018, **126**, 353–362.
- 41 N. H. Abu-Hamdeh, R. A. R. Bantan, A. Golmohammadzadeh and D. Toghraie, *J. Mol. Liq.*, 2021, **325**, 115149.
- 42 V. M. Nazarychev, A. D. Glova, I. V. Volgin, S. V. Larin, A. V. Lyulin, S. V. Lyulin and A. A. Gurtovenko, *Int. J. Heat Mass Transfer*, 2021, **165**, 120639.
- 43 D. Surblyis, H. Matsubara, G. Kikugawa and T. Ohara, *Phys. Rev. E*, 2019, **99**, 051301.
- 44 A. Pereverzev and T. Sewell, *Int. J. Heat Mass Transfer*, 2022, **188**, 122647.
- 45 P. Boone, H. Babaei and C. E. Wilmer, *J. Chem. Theory Comput.*, 2019, **15**, 5579–5587.
- 46 V. M. Nazarychev, A. D. Glova, S. V. Larin, A. V. Lyulin, S. V. Lyulin and A. A. Gurtovenko, *Int. J. Mol. Sci.*, 2022, **23**, 14576.
- 47 J. B. Klauda, R. M. Venable, J. A. Freites, J. W. O'Connor, D. J. Tobias, C. Mondragon-Ramirez, I. Vorobyov, A. D. MacKerell and R. W. Pastor, *J. Phys. Chem. B*, 2010, **114**, 7830–7843.
- 48 J. B. Klauda, B. R. Brooks, A. D. MacKerell, R. M. Venable and R. W. Pastor, *J. Phys. Chem. B*, 2005, **109**, 5300–5311.
- 49 A. D. Glova, S. V. Larin, V. M. Nazarychev, J. M. Kenny, A. V. Lyulin and S. V. Lyulin, *ACS Omega*, 2019, **4**, 20005–20014.
- 50 D. Chen, T. S. Totton, J. W. J. Akroyd, S. Mosbach and M. Kraft, *Carbon*, 2014, **67**, 79–91.
- 51 A. D. Glova, I. V. Volgin, V. M. Nazarychev, S. V. Larin, S. V. Lyulin and A. A. Gurtovenko, *RSC Adv.*, 2019, **9**, 38834–38847.
- 52 I. V. Volgin, A. D. Glova, V. M. Nazarychev, S. V. Larin, S. V. Lyulin and A. A. Gurtovenko, *RSC Adv.*, 2020, **10**, 31316–31317.
- 53 B. Hess, *J. Chem. Theory Comput.*, 2008, **4**, 116–122.
- 54 U. Essmann, L. Perera, M. L. Berkowitz, T. Darden, H. Lee and L. G. Pedersen, *J. Chem. Phys.*, 1995, **103**, 8577.

- 55 S. Plimpton, *J. Comput. Phys.*, 1995, **117**, 1–19.
- 56 D. Van Der Spoel, E. Lindahl, B. Hess, G. Groenhof, A. E. Mark and H. J. C. Berendsen, *J. Comput. Chem.*, 2005, **26**, 1701–1718.
- 57 J. Lee, X. Cheng, J. M. Swails, M. S. Yeom, P. K. Eastman, J. A. Lemkul, S. Wei, J. Buckner, J. C. Jeong, Y. Qi, S. Jo, V. S. Pande, D. A. Case, C. L. Brooks, A. D. MacKerell, J. B. Klauda and W. Im, *J. Chem. Theory Comput.*, 2016, **12**, 405–413.
- 58 S. Jo, T. Kim, V. G. Iyer and W. Im, *J. Comput. Chem.*, 2008, **29**, 1859–1865.
- 59 M. R. Shirts, C. Klein, J. M. Swails, J. Yin, M. K. Gilson, D. L. Mobley, D. A. Case and E. D. Zhong, *J. Comput.-Aided Mol. Des.*, 2017, **31**, 147–161.
- 60 W. Humphrey, A. Dalke and K. Schulten, *J. Mol. Graphics*, 1996, **14**, 33–38.
- 61 D. Andrienko, V. Marcon and K. Kremer, *J. Chem. Phys.*, 2006, **125**, 124902.